Comparison of the structural dynamic and mitochondrial electron-transfer properties of the proapoptotic human cytochrome *c* variants, G41S, Y48H and A51V

Oliver M. Deacon[1], Richard W. White[1], Geoffrey R. Moore[2], Michael, T. Wilson[1], Jonathan A.R. Worrall[1]*

[1]School of Life Sciences, University of Essex, Wivenhoe Park, Colchester, CO4 3SQ, UK.
[2]School of Chemistry, University of East Anglia, Norwich Research Park, Norwich, NR4 7TJ, UK.

To whom correspondence may be addressed:
Jonathan A.R. Worrall; jworrall@essex.ac.uk

ABSTRACT

Mitochondrial cytochrome c is associated with electron transfer in the respiratory chain and in apoptosis. Four cytochrome c variants have been identified in families that suffer from mild autosomal dominant thrombocytopenia, a platelet disorder associated with increased apoptosis. Three out of the four substitutions, G41S, Y48H and A51V are located on the 40-57 Ω-loop. The G41S and Y48H variants perturb key physicochemical and dynamic properties that result in enhanced functional features associated with apoptotic activity. Herein we characterise the ferric A51V variant. We show by chemical denaturation that this variant causes the native state to be destabilized. Through azide binding kinetics, the population of a pentacoordinate heme form, whereby the Met80 axial ligand is dissociated, is estimated to be of equal magnitude to that found in the Y48H variant. This pentacoordinate form gives rise to peroxidase activity, which despite the similar pentacoordinate population of the A51V variant to that of the Y48H variant, the peroxidase activity of the A51V variant is supressed. Far-UV circular dichroism spectroscopy and pH jump studies, suggest that a combination of structural and dynamic features in addition to the population of the pentacoordinate form regulate peroxidase activity in these disease variants. Additionally, the steady-state ratio of ferric/ferrous cytochrome c when in turnover with cytochrome c oxidase has been investigated for all 40-57 Ω-loop variants. These studies show that the lower pK_a of the alkaline transition for the disease causing variants increases the ferric to ferrous heme ratio, indicating a possible influence on respiration *in vivo*.

Key words: Cytochrome c, apoptosis, respiration, peroxidase, pH jump, cytochrome c oxidase

INTRODUCTION

Mitochondrial cytochrome *c* (Cc) is a key protein in the life and death processes of a eukaryotic cell. In humans, it is now widely recognised that Cc has an extensive repertoire of roles ranging from acting as an electron shuttle in oxidative phosphorylation to roles in apoptosis, redox signalling, as an inhibitor of histone chaperone activity and an involvement in the mitochondrial oxidative folding machinery.[1-4] These multiple functions have led to Cc being branded as an extreme multifunctional (EMF) protein.[5, 6]

Cc possesses a hexacoordinate heme, with axial heme iron coordination derived from the $N^{\delta 1}$ atom of His18 and the S^{γ} atom of Met80.[7] The *c*-type heme is bound to the polypeptide through a CXXCH motif within a fold that comprises of five α-helices, and three Ω-loops[7] (structural motifs with residues at the start and end of the loop close in space [8, 9]). Embedded in the EMF persona of Cc is its ability to access energetically favoured conformational states above its ground state native structure.[5] Under physiological conditions the ferric form of Cc exists in an equilibrium between the dominant hexacoordinate form and a minor populated pentacoordinate state, in which the Met80 ligand is dissociated from the heme iron.[7] Despite the pentacoordinate population being exceedingly low, it is sufficient to confer peroxidase activity,[10-15] which has implications for apoptotic activity, in particular when Cc is complexed with the phospholipid cardiolipin (CL).[16-24]

At alkaline pH, ferric Cc can access a conformational state whereby a deprotonation of a group within a hydrogen bonded network of amino acid side chains and a heme propionate causes dissociation of the Met80 ligand [25] and subsequent coordination to the heme iron by a Lys residue from the 71-85 Ω-loop.[25-28] This transition is commonly referred to as the alkaline transition and when measured under equilibrium conditions has an apparent pK_a of ~ 9 depending on solution conditions and Cc species.[7, 29, 30] A common feature in formation of these non-native conformers of ferric Cc is a dynamic communication between the 40-57 and 71-85 Ω-loops.[5, 25, 31, 32] These two structural units have been shown to possess the lowest free energy out of the five cooperative folding/unfolding units (foldons) assigned in Cc, with the 40-57 Ω-loop having the lowest stability.[33-36] Furthermore, the Fe(III)-Sγ(Met80) bond strength, a key regulator to accessing the non-native states, is influenced by an entatic contribution of the protein derived through a hydrogen bonding network that communicates between the two Ω-loops.[37] Perturbation of this hydrogen bonding network diminishes the entatic control and enhances Met80 dissociation.[25, 37]

Four pathogenic mutations in the human Cc gene have been identified in families that suffer from mild autosomal dominant thrombocytopenia (THC4; OMIM 612004); a disorder caused by dysregulated platelet formation associated with increased mitochondrial apoptosis.[38-41] Three of the mutations are missense and give rise to the G41S, Y48H and A51V variants found in the 40-57 Ω-loop,[38-40] with the fourth an in-frame deletion that results in a variant whereby Lys100 in the C-terminal α-helix is deleted[41] (Fig. 1). The G41S variant possesses enhanced apoptotic activity *in vitro*,[38] with subsequent studies providing further insights into the physicochemical properties inherent in this variant attributing to enhancing apoptotic activity.[23, 24, 31, 42, 43] Of particular note is an increased population of the pentacoordinate heme form under non-denaturing conditions.[23, 31] Enhanced apoptotic activity of the Y48H variant was initially reported,[39] with a more detailed *in vitro* characterisation revealing the Y48H variant to have substantially higher peroxidase activity than the G41S variant, attributed to the equilibrium between the hexacoordinate and pentacoordinate heme forms being shifted further towards the pentacoordinate state.[5] Solution NMR spectroscopy studies on these variants demonstrated that main chain dynamics were enhanced compared to wild-type (WT) human Cc (hCc).[5, 31] Notably, the dynamic hot spots are centred around the 40-57 and 71-85 Ω-loops with a dynamic hierarchy of Y48H > G41S > WT, which currently scales with the population of the pentacoordinate species associated with peroxidase activity.[5, 31]

In the present study we have prepared the A51V variant to ascertain the properties this mutation infers on the functional properties of hCc and to place the findings in context with our previous studies with the G41S and Y48H variants.[5, 25, 31] We have performed a suite of experiments designed to probe the pentacoordinate form of the native state that gives rise to the peroxidase activity. We find that the A51V variant has a relatively mild effect on the physicochemical properties of hCc. However, despite the population of the pentacoordinate heme species being enhanced, the peroxidase activity remains supressed compared to the G41S and Y48H variants. Furthermore, we have investigated the effects of the three 40-57 Ω-loop variants on the redox state of hCc in steady-state turnover with cytochrome *c* oxidase (CcO). In these turnover experiments the redox state of hCc was affected by the nature of the substitution, with Y48H having the larger effect and the A51V the least.

MATERIALS AND METHODS

Construction of the A51V hCc variant

The A51V variant of hCc was constructed using the Quikchange mutagenesis (Stratagene) protocol with the pUC19hCc plasmid as template.[23] The forward and reverse mutagenic primers were as follows: 5'-CTCTTACACAGCCGtgAATAAGAACAAAG 3' and 5'-CTTTGTTCTTATTcaCGGCTGTGTAAGAG-3', respectively, with the mutation sites in lower case. A PCR mix consisting of primers (75 ng/µl), pUC19hCc (15 ng/µl), 10 mM dNTPs (Fermentas), Pfu (*Pyrococcus furiosus*) Turbo polymerase (Agilent), 10x polymerase buffer (Agilent) and deionised water to give a final volume of 50 µl and subjected to the following PCR cycle; 95 °C – 3 min, (95 °C – 1 min, 65 °C – 1 min, 72 °C – 6 min) x 18, 72 °C – 10 min. PCR products were digested with the restriction enzyme *DpnI* (Fermentas) and transformed into *Escherichia coli* XL1-Blue (Agilent) cells. DNA sequencing was used to confirm the presence of the desired nucleotide changes (Source BioScience, UK).

Over-expression of hCc and variants

Over-expression of WT hCc, the G41S, Y48H and A51V variants was carried out in *E. coli* strain BL21(DE3)-RIL (Agilent) with isolation and purification of all proteins as reported previously.[23]

Isolation and purification of bovine CcO

A fresh bovine heart was obtained from C.J. Byford & Sons (Clacton-on-Sea, U.K.) and CcO was isolated according to a previously reported procedure.[44] The pure CcO, as judged by the absorbance ratio 445/420 nm in the reduced state of > 2.5, was aliquoted and stored in 100 mM potassium phosphate, pH 7.4, 1% Tween80 (Sigma-Aldrich) at -80 °C until required.

Protein preparation

Oxidized Cc proteins were prepared by the addition of excess $K_3[Fe(CN)_6]$, followed by removal of $K_3[Fe(CN)_6]$ and $K_4[Fe(CN)_6]$ and exchanged into a desired buffer using a PD-10 column (GE Healthcare). Protein concentrations were determined using a Cary 60 spectrophotometer (Agilent). Molar extinction coefficients (ε) were determined for ferric WT hCc and variants using a pyridine hemochromogen assay[45] and are reported in Table S1. Aliquots of CcO were thawed and spun for 2-3 min at high speed in a micro-centrifuge. The absorbance peak at 605 nm ($\varepsilon = 21,000$ M^{-1} cm^{-1}) in the reduced CcO samples arising from heme *a* was used to determine sample concentration. All CcO concentrations are expressed in terms of heme *a* concentration.

Far-UV circular dichroism spectroscopy and chemical denaturation

Far-UV circular dichroism (CD) spectroscopy was carried out using an Applied Photophysics Chirascan CD spectrophotometer (Leatherhead, UK) thermostatted at either 15 or 20 °C. Ferric protein samples (18-26 μM) were prepared in 10 mM potassium phosphate, 50 mM potassium fluoride pH 6.5 and a wavelength scan between 190-250 nm was conducted. To determine protein stability, a 6 M stock solution of guanidine hydrochloride (GuHCl) (Fluka) was prepared in the identical buffer and titrated into a ferric A51V variant sample. Changes in molar ellipticity at 222 nm (θ_{222nm}) were monitored and the free energy of unfolding (ΔG_{unf}) and dependence of ΔG_{unf} on denaturant concentration (*m*-value) were calculated using equation 1 [46]

$$\theta_{222nm} = \frac{(\alpha_N + \beta_N[GuHCl]) + (\alpha_D + \beta_D[GuHCl])\exp(\frac{-\Delta G_{unf} + m[GuHCl]}{RT})}{1 + \exp(\frac{-\Delta G_{unf} + m[GuHCl]}{RT})} \qquad (1)$$

where α_N and α_D correspond to the baseline values of the native and denatured protein at 0 M GuHCl respectively, and β_N and β_D to their respective dependence on [GuHCl] *i.e.* the slope. ΔG_{unf} is the free energy of denaturation in water and *m* represents the dependence of the free energy of denaturation on [GuHCl]. To represent the data in terms of fraction denatured (F_D) at any given [GuHCl] equation (2) was used.[47]

$$F_D = \frac{\theta_{222nm} - (\alpha_N + \beta_N[GuHCl])}{(\alpha_D + \beta_D[GuHCl]) - (\alpha_N + \beta_N[GuHCl])} \qquad (2)$$

All titrations were carried out in triplicate with the errors reported the standard error.

Alkaline pH titrations

The pH dependence of the 695 nm band in the electronic absorption spectrum of the ferric A51V hCc variant (100 μM) was monitored at 25 °C by determining the absolute absorbance at various values of pH in the presence of a small aliquot of $K_3[Fe(CN)_6]$ to maintain an oxidising environment. The pH of the buffer (20 mM sodium phosphate pH 6.0) was adjusted with microliter aliquots of 1 M NaOH and measured after each addition using a semi-micro glass pH electrode. pH titrations were repeated three times and with different batches of

proteins. Data were fitted to a one-proton ionization equilibrium equation to yield an apparent pK_a.

Peroxidase assays

The oxidation of 2,2-Azinobis(3-ethylbenthiazoline-6-sulfonic acid) (ABTS; Fisher) was monitored at 730 nm on a Hewlett-Packard 8453 diode-array spectrophotometer scanning between 190 and 1100 nm and thermostatted at 20 °C. The reaction was initiated by the addition of 1 mM H_2O_2 (after 40 s) to a series of cuvettes containing 5 µM of the ferric A51V variant and 200 µM ABTS. Using the wavelength pair 475-730 nm the slope of each trace (post-lag phase) was determined to obtain a rate in AU/s. The turnover rate is reported in s^{-1} obtained by dividing AU/s by the product of the concertation of oxidized ABTS ($\varepsilon = 14$ mM^{-1} cm^{-1}) and the total protein concentration (5 µM). All assays were carried out in triplicate with errors reported as the standard error.

Azide binding kinetics

An Applied Photophysics (Leatherhead, UK) SX20 stopped-flow spectrophotometer thermostatted at 25 °C and equipped with both photomultiplier and diode array detection systems was used to monitor rapid reaction kinetics. A stock solution of 2 M sodium azide (N_3^-; Sigma-Aldrich) was buffered in 50 mM 2-(N-morpholino)ethanesulfonic acid (MES) pH 7.0 and diluted to the desired $[N_3^-]$ with the same buffer containing 2 M NaCl to maintain the ionic strength. Reaction time-courses were taken at 420 nm with $[N_3^-]$ varying between 0.08 and 2 M (before mixing) and 10 µM protein (before mixing). All transients were fitted to a single exponential function yielding both pseudo first-order rate constants and amplitudes. Assuming N_3^- binding to ferric Cc is an SN_1 mechanism, in which the hexacoordinate heme form is in equilibrium with a pentacoordinate form, the latter being the form that binds N_3^-, then, as outlined previously,[31] equations 3 and 4 may be derived that describe the K_{app} and the dependence of k_{obs} for N_3^- binding as a function of $[N_3^-]$.

$$K_{app} = K_D\left(\frac{K+1}{K}\right) \qquad (3)$$

$$k_{obs} = \frac{(k_1 - k_{-2})[N_3^-]}{\left(\frac{k1+k_{-1}}{k'}\right)+[N_3^-]} + k_{-2} \qquad (4)$$

In these equations, $K = k_1/k_{-1}$, where k_1 and k_{-1} are the rate constants for Met80 dissociation and association respectively and $K_D = k_{-2}/k_2$, with k_2 the pseudo-first order rate constant for N_3^- binding *i.e.* $k_2 = k'[N_3^-]$, where k' is the second order rate constant and k_{obs} is ~ k_1 at high $[N_3^-]$. The data for the A51V and Y48H variants were not collected over a sufficiently wide range to allow for the fitting algorithm to converge and yield values for the three parameters defining equation 4. However, convergence was achieved to yield values of k_{-2} (the intercept on the ordinate), which was then fixed and not allowed to vary, to determine k_1 with its associated errors. In addition calculation of k_1 using either the upper or lower bound error for k_{-2} were used and these values are discussed in the footnote to Table 2.

pH jump kinetics

For pH jumping experiments a range of pH buffers containing 50 mM KCl, 50 mM boric acid (pH 7 - 9) or 50 mM N-cyclohexyl-3-aminopropanesulfonic acid (CAPS) (pH 9 - 13) were prepared and stocks of the ferric A51V variant prepared in H_2O and diluted to experimental concentrations in 50 mM KCl, to maintain ionic strength during mixing, to a pH of ~ 7. pH jump experiments were initiated in a stopped-flow spectrophotometer by mixing solutions of the ferric A51V variant with an equal volume of high pH buffer. First order rate constants (k_{obs}) were obtained by fitting reaction time-courses to either a single exponential at pH values between 8.5 and 10 (k_{obs1} slow phase) or at pH values above 10.5 a double exponential function (k_{obs1} and k_{obs2} fast phase). Experiments were repeated in triplicate and with different protein batches with errors reported the standard error. All kinetic analysis was conducted using the software ProKineticist (Applied Photophysics).

Turnover experiments using cytochrome c oxidase

Kinetic experiments were carried out using a stopped-flow spectrophotometer operating in photo diode array mode. CcO (5 µM), ferric h Cc (20 µM), sodium ascorbate (10 mM; Sigma-Aldrich) and the redox mediator *N,N,N',N'*-tetramethyl-p-phenylenediamine (TMPD concentrations ranging between 100 to 600 µM; Fisher) were dissolved in 0.1 M sodium phosphate buffer, pH 7.4, containing 1% Tween 80 (Sigma-Aldrich). This solution rapidly exhausts the oxygen present in solution and fully reduces both the Cc and CcO (cyt *aa₃* Cu_A Cu_B) before rapidly mixing with aerobic buffer (~270 µM oxygen as determined from the solubility coefficient using the temperature and pressure on the day). On mixing, the reduced CcO is fully oxidised within the dead time of the stopped-flow (~ 1.5 ms) and thereafter a sequence of reactions occur (see Results) that leads eventually to the complete depletion of

oxygen and the return of the system to the fully reduced state. The excursions of the spectral absorption bands associated with the chromophores present were followed using a diode array accessory and time courses and levels of reduction in steady-state monitored.

RESULTS

Far-UV CD spectroscopy of the ferric A51V variant and comparison with the G41S and Y48H hCc variants

The far-UV CD profile for ferric hCc is shown in Figure 2A, with the characteristic minima at 208 and 222 nm consistent with a fully folded protein dominated by α-helical structure. The ferric A51V variant displays a similar profile, as do the G41S and Y48H variants, confirming in the first instance that on purification the A51V variant is folded (Fig. 2A). No differences in the far-UV CD profiles for the WT or any of the variants in a temperature range between 10 and 30 $^{\circ}$C were observed (data not shown). The X-ray structures of the three variants, [5, 42, 48], reveal no significant secondary structure differences in respect to the WT structure.[23] In contrast, solution NMR studies indicate that the G41S and Y48H variants are more dynamic than the WT protein.[5, 31] In this respect, we note that the $\theta_{222/208\,nm}$ ratio between the variants varies from the WT protein (Fig. 2A). For the WT protein, the $\theta_{222/208\,nm}$ ratio is 1.3, with a value of 1.1 determined for the G41S and A51V variants and the Y48H variant having a ratio of 0.9. For a globular α-helical protein, perturbations to the $\theta_{222/208\,nm}$ ratio can be associated with changes in interhelical interactions resulting from changes to the packing of Trp side chains within a protein core [49]. In Cc, Trp59 has a key role in the packing of the Cc hydrophobic core.[50] Therefore, the $\theta_{222/208\,nm}$ ratio hierarchy (WT > G41S $\cong$ A51V > Y48H) may infer differences in packing around Trp59, arising from the increased global dynamics reported from NMR studies for the G41S and Y48H variants,[5, 31] and therefore a similar increase in dynamics could be anticipated for the A51V variant.

Global stability of the ferric A51V hCc variant

The thermodynamic unfolding parameters for the ferric A51V variant were obtained by monitoring the decrease in θ at 222 nm in the far-UV CD spectrum upon titration with GuHCl. The conditions employed (pH 6.5 and 15 $^{\circ}$C) were identical to those used previously for the G41S and Y48H variants for which the free energy changes were used in conjunction with NMR H/D-exchange data collected at 15 $^{\circ}$C.[5] Table 1 reports the ΔG_{unf}, *m*-value and C_m values for the ferric A51V variant and a plot of the fraction unfolded versus [GuHCl] is shown

in Fig. 2B. It is apparent from Table 1, that the global stability of the ferric A51V variant follows a similar trend to both the G41S and Y48H variants, in that the cooperativity of unfolding (*m*-value) decreases, leading to a decrease in the ΔG_{unf}, with respect to WT hCc. As noted previously,[5] the introduction of a His residue in the Y48H variant has connotations to the possibility of it competing with His26 and His33 in ligating to the heme iron in the denatured state. Therefore, a comparison of the stability ($\Delta\Delta G_{unf}$) amongst the three variants is made using GuHCl at a pH where additional competing misligation in the denatured state for the Y48H protein is a possibility (Table 1). However, from the $\Delta\Delta G_{unf}$ a hierarchy of global stability for the 40-57 Ω-loop variants of WT >> A51V $\cong$ G41S >> Y48H is observed, with a parity between the A51V and G41S variants and the Y48H variant being the outlier.

Effect on the local stability of the 71-85 Ω-loop imposed by the A51V hCc variant

From previous work with the ferric G41S and Y48H variants, we have shown that mutations in the 40-57 Ω-loop influence the structural dynamics of the Met80-containing Ω-loop, with consequences for the Fe(III)-Sγ(Met80) bond lability.[5, 31] Our preference has been to investigate the local dynamics of the 71-85 Ω-loop by using the kinetics of N_3^- binding.[5, 25, 31] Such experiments provide an insight into the population of the pentacoordinate heme form *i.e.* the Met80-off form that binds N_3^- and gives rise to the intrinsic peroxidase activity. Upon mixing N_3^- with the ferric A51V variant, an optical transition occurs caused by dissociation of the Met80 ligand from the heme iron and binding of N_3^- in its place.[31] The reaction time-course of this transition for the A51V variant conformed to a simple exponential as reported for other hCc variants under identical experimental conditions. [5, 25, 31] The normalised amplitudes of the reaction time-courses over a broad range of [N_3^-] follows a simple hyperbolic relationship, enabling an apparent equilibrium constant (K_{app}) for N_3^- binding to be determined (Fig. 3A). The K_{app} for the ferric A51V variant is reported in Table 1, together with K_{app} values for the ferric forms of the G41S and Y48H variants.[5, 31] Notably, the A51V variant has a K_{app} identical to the Y48H variant. The relationship between the rate constant for N_3^- binding (k_{obs}) and [N_3^-] given in equation 4 should conform to a hyperbola, where a curve is expected to reach a plateau (*i.e.* k_1, the Met80 ligand dissociation rate constant). As previously discussed for WT hCc and the G41S and Y48H variants this is not the case under the conditions employed, as a suitably high [N_3^-] cannot be explored.[5, 25, 31] Earlier work using linear fitting procedures used reciprocals to obtained k_1 values of 30 s^{-1} for horse heart Cc using N_3^- as the competing ligand.[51] Refitting of this earlier data using equation 4 (non-linear fitting)

gives a value of between 11-16 s^{-1} for horse heart Cc [31] which is comparable to that of WT hCc (Table 1). A non-linear fit to the data for the A51V variant is shown in Figure 3B and yields the k_1 and k_{-2} values reported in Table 1. A comparison of the k_1 and k_{-2} values reported previously for the WT, G41S and Y48H variants reveals the k_1 of the Met80 ligand for the A51V variant is elevated above the WT hCc and lies closer to the G41S variant, rather than the Y48H variant (Table 1).

Equation 3 shows that when $K < 1$, as seen here, because the concentration of the pentacoordinate species is low, then K_{app} is $\sim K_D/K$. Based on the assumption that N$_3^-$ binding to the pentacoordinate heme species is not influenced directly by the different substitutions in the protein other than by the provision of pentacoordinate ferric heme, then K_D will be similar for all proteins in Table 1, so that the ratio of K_{app} values in $^{WT}K_{app}/^{variant}K_{app}$, reflects the ratio of K values $^{variant}K/^{WT}K$ and therefore is indicative of the relative proportions of the pentacoordinate heme state. We have justified the assumption that the heme in the WT hCc and variants have the same intrinsic K_D in our previous work and have proposed that the differences between the WT and variants reflect the different extent to which the protein matrix cages the heme group from the approach of the ligands.[25] This justification is based on the fact that the measured off-rate of the N$_3^-$ (k_{-2}) and the Met80-off rate (k_1) for the disease variants conforms to a hyperbola, asymptotic to 11.8 ± 0.6 s^{-1} (Fig. 3C). As this value is only reached when Met80 is essentially dissociated it constitutes the intrinsic dissociation rate constant, k_{-2} intrinsic, of N$_3^-$ dissociating from the heme in these hCc variants. As the A51V variant falls neatly on the same hyperbolic relationship we conclude this variant likewise has the same intrinsic K_D (Fig. 3C). Therefore based on these previous arguments,[25] the A51V variant has a pentacoordinate heme state populated to essentially the same extent as the Y48H variant as determined from N$_3^-$ binding kinetics (*i.e.* $^{variant}K/^{WT}K$).

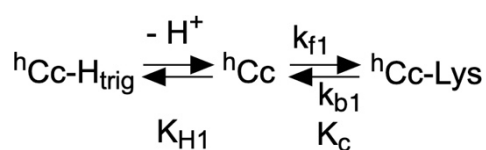*Peroxidase activity of the A51V hC c variant*

The intrinsic peroxidase activity of Cc arises from the existence of an equilibrium in the ferric heme state between the hexacoordinate Met80-bound form and a pentacoordinate Met80-off form, with the latter being peroxidase active.[7, 10-15] In the early stages of apoptosis, CL complexes with Cc, resulting in the pentacoordinate form becoming dominant, enabling oxidation of CL to occur.[16] A feature of the 40-57 Ω-loop variants has been their increased intrinsic peroxidase activity relative to WT hCc.[5, 23, 24] Under identical assay conditions to previous studies with the G41S and Y48H variants,[5] the A51V variant is capable of oxidizing

ABTS in the presence of H_2O_2, with a turnover lower than that of the G41S variant, but greater than for the WT protein (Fig. 4). Notably, the apparent equivalent population of the pentacoordinate species for the A51V and Y48H variants deduced from N_3^- binding kinetics does not manifest itself in the intrinsic peroxidase activity of these two variants (Fig. 4), with the A51V variant having peroxidase activity closer to the WT and G41S variant than the Y48H variant.

Alkaline isomerisation and pH jump kinetics of the ferric A51V hCc variant

The 695 nm absorbance band in the electronic absorption spectrum of ferric hCc reports on the presence of the Met80(Sγ)-Fe(III) heme bond.[7, 52] It is well established that as the pH increases towards alkalinity, a bleaching of the 695 nm band is observed that is a consequence of the dissociation of a single proton resulting in the dissociation of the Met80 heme ligand and replacement by a Lys residue found in the 71-85 Ω-loop.[25-28, 53] The Lys bound form of Cc is referred to as the alkaline conformer.[53] For the A51V variant the apparent pK_a for the alkaline conformer, determined by monitoring the bleaching of the absorbance band at 695 nm is 8.3 ± 0.1 (Fig. 5A), similar to the decrease of ~ 1 pH unit compared with WT hCc seen with the G41S and Y48H variants (Table 2). Thus, the three disease causing variants each stabilize the alkaline conformer to a similar degree relative to the WT protein.

The kinetics of the alkaline transition in mitochondrial Cc have been extensively studied and the mechanistic features can be described by a simple model depicted in Scheme 1, whereby deprotonation of a group termed the trigger (pK_{H1}), initiates a conformational change that leads to the substitution of the Met80 ligand with a Lys residue.[54]

$$^hCc\text{-}H_{trig} \underset{K_{H1}}{\overset{-H^+}{\rightleftharpoons}} {}^hCc \underset{k_{b1}}{\overset{k_{f1}}{\rightleftharpoons}} {}^hCc\text{-}Lys$$
$$K_c$$

Scheme 1

In Scheme 1, ^hCc-H_{trig} depicts the His/Met hexacoordinate protein with the trigger protonated, ^hCc the His/Met hexacoordinate protein with the trigger deprotonated, and ^hCc-Lys the hexacoordinate alkaline conformer of Cc with Lys now coordinated. K_{H1} and K_c are the equilibrium constants for the protonation/deprotonation and the conformational change, respectively, and k_{f1} and k_{b1} are the forward and backward rate constants, respectively. The ferric A51V variant was subjected to a series of stopped-flow pH jump experiments in the pH
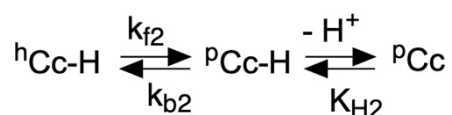
range 7.0 to 10.0. where a single spectral transition was observed with the Soret band blue-shifted and the 695 nm band bleached. We have adopted an analysis in which the full data set is subjected to singular value decomposition with no evidence for more than one phase. The transition therefore could be adequately fitted to a single exponential phase, with the determined rate constants (k_{obs1}) increasing as expected with increasing pH (Fig. 5B). Similar behaviour has been previously reported for WT hCc and the G41S and Y48H variants.[25] Based on the model in Scheme 1, equation 5

$$k_{obs1} = k_{b1} + k_{f1}\left(\frac{K_{H1}}{K_{H1}+H^+}\right) \quad\quad\quad (5)$$

can be used to fit the titration curve displayed by the A51V variant in Fig. 5B to yield the pK_{H1} of the trigger. In equation 5, k_{obs1} takes the value k_{b1} at low pH and $k_{b1} + k_{f1}$ at high pH values. The k_{f1} and pK_{H1} values for the A51V variant determined from the experimental data are reported in Table 2, and k_{b1} values have been estimated due to the difficulties in directly obtaining accurate values (as was also the case in previous work[25]). Comparison of the k_{f1} and pK_{H1} values for the A51V variant with those determined for WT hCc and the G41S and Y48H variants are reported in Table 2, where it is apparent that the A51V variant lowers the pK_{H1} of the trigger by > 1 pH unit as noted with the other disease associated variants.[25] However, the pK_{H1} value for the A51V variant is slightly higher relative to the G41S and Y48H variants, but nevertheless continues the trend of substitutions in the 40-57 Ω-loop for making the trigger substantially easier to deprotonate.

At higher pH values (> 10) a second rapid phase (k_{obs2}), in addition to the slow phase (k_{obs1}) has been reported for hCc, several of its variants and horse heart Cc.[25, 55-58] For the A51V variant this rapid phase is also observed (Fig. 6A). The rate constant, k_{obs2}, is associated with the formation of a transient spectrum characteristic of a high-spin (HS) ferric heme species having a prominent band at ~ 600 nm (Fig. 6B) and possessing long wavelength features that obscure the bleaching of the 695 nm band at some pH values. The spectrum decays to a final low-spin form typical of a ferric heme species with a Lys/His coordination (Fig 6B). It is notable for the A51V variant that this HS species is populated to a lesser extent than either the G41S and Y48H variants.[25] The k_{obs2} values decrease for the A51V variant until ~ pH 11, before rising steeply (Fig. 5C). At the lower pH values, the decrease in k_{obs2} values observed for the A51V variant is reminiscent of the WT protein (Fig. 5C), rather than the G41S and Y48H variants, where k_{obs2} values increase from pH 10 and above (Fig. 5C). Above pH 11 the

A51V variant behaves as the G41S and Y48H variants. The increasing k_{obs2} values for the G41S and Y48H variants implies that deprotonation precedes the conformational change that leads to the dissociation of the Met80 ligand from the heme iron.[25] This behaviour has been assigned to a coupling between a conformational change that exposes a group (not the trigger) that then undergoes deprotonation leading to the stabilization (or facilitation) of a HS heme species,[57] as represented in Scheme 2.

$$^{h}Cc\text{-}H \; \underset{k_{b2}}{\overset{k_{f2}}{\rightleftharpoons}} \; ^{p}Cc\text{-}H \; \underset{K_{H2}}{\overset{-H^{+}}{\rightleftharpoons}} \; ^{p}Cc$$

Scheme 2

In Scheme 2, -H represents the non-exposed group in the hexacoordinate His/Met form (^{h}Cc-H) and the exposed group (after conformational change) in the pentacoordinate ^{p}Cc-H form, with ^{p}Cc representing the deprotonated HS heme form. Thus the A51V variant appears to be a combination of both the WT hCc (in the lower pH range) and the G41S and Y48H variants in the higher pH range, except that the pK_{H2} calculated for the G41S and Y48H variants of 11.0 [25] is shifted to a higher value (~ 11.5) for the A51V variant. It should be noted for WT hCc the pK_{H2} cannot be calculated as the k_{obs2} values obtained at pH values > 12.5 are obscured by a more general denaturation of the protein as commented on previously.[25]

Steady-state kinetics of CcO with the three THC4 causing 40-57 Ω-loop variants

The respiratory function of Cc requires it to carry an electron from cytochrome *c* reductase (complex III) and deliver it to CcO (complex IV). Electrons enter the dinuclear Cu_A site of CcO and are passed to heme *a* and then to heme a_3 and finally Cu_B, where a dioxygen molecule is reduced coupled to proton pumping across the membrane.[59, 60] At physiological pH, one might expect that lowering the pK_a value from ~ 9.3 (WT hCc [5]) to ~ 8.4 (G41S and Y48H variants [5]) would lead to an increase in the fraction of the ferric Cc in the alkaline, non-reducible form, and therefore to a change in the steady-state ratio of ferric/ferrous Cc when this is in turnover with its natural partner, CcO. To assess whether this is the case for the disease variants a series of steady-state experiments have been undertaken. These experiments monitor the redox state of WT hCc and variants while in turnover, receiving electrons from ascorbate/TMPD and donating these electrons to CcO and thence to oxygen. The methodology employed ensures that fully oxidised, activated ("pulsed") CcO is presented with fully reduced

14

hCc in the presence of oxygen and a reductant system (sodium ascorbate and the mediator TMPD).[61] Figure 7A shows the result of such an experiment and displays spectra collected at known times. By increasing the rate of WT hCc reduction by ascorbate through addition of higher concentrations of TMPD, the steady-state reduction level of the whole system may be adjusted (Fig. S1). In Fig. 7A the spectra shown demonstrate that initially WT hCc is fully reduced and then rapidly donates electrons to oxidized CcO. The system now enters into steady-state (between 2 - 22 s) in which hCc is held at ~ 40 % reduced during turnover (Fig. 7A and Fig. S1). Once the oxygen present is depleted, WT hCc (and CcO) is returned to the fully reduced state (31 s) by the excess reductant (Fig. 7A). The time course followed at 550 nm, the α band of ferrous hCc, is shown in Figure 7B and reports that the redox state of hCc remains almost constant between 2 and 22 s, *i.e.* from the time the system enters steady-state until oxygen is exhausted (Fig. 7B). Closer examination, however, reveals that during this time there is a small decrease in the level of reduced WT hCc. This is better seen in the difference spectra shown in Fig. 7C in which the spectrum collected at 22 s is subtracted from that collected at 2 s. This difference spectrum is that of reduced minus oxidised WT hCc and shows that approximately 1.5 % of the protein became ferric in the time of the steady-state (between 2 and 22 s).

The same experiment was conducted using the G41S, Y48H and the A51V variants, and gave similar overall results but showed that in the variants the shift towards the ferric form was enhanced. This can be appreciated from Figure 8, where the difference spectra (between the start and end of the steady-state as illustrated in Fig. 7B) are compared for all variants. A clear trend in the drift toward the ferric form during steady-state may be discerned, in the order of Y48H (9.5 %) > G41S (3.5 %) > A51V (2.2 %) > WT (1.5 %). This order is the same as that already seen in the values of the Met80 dissociation rate constants (k_1) determined from N_3^- binding kinetics (Table 1).

DISCUSSION

The A51V substitution is located in a regular secondary structure motif (α2-helix), in contrast to the disease causing mutations at the 41 and 48 positions, which lie on a region of the 40-57 Ω-loop devoid of secondary structure (Fig. 1). The α2-helix in hCc has the sequence TAA[51]NKNK, with Ala51 found at the N + 3 position. It is well documented that Ala has the highest helix propensity and is thus the most stabilising residue within an α-helix.[62] Val on the other hand is considered to be a destabilizing residue in an α-helix, with an estimated free

energy difference ($\Delta\Delta G$) from Ala (which is arbitrarily set at $\Delta G = 0.0$ kcal/mol) of 0.61 kcal/mol.[62] This destabilizing effect arises from an unfavourable change in side-chain conformational entropy when a helix is formed, with the loss greatest for amino acids with branched β-carbons allowing only the *trans* conformation in folded states.[63, 64] Globally, at least, the Ala to Val mutation causes the native structure to be destabilised to a similar degree as the G41S variant (Table 1), with the decreasing $\theta_{222/208 \text{ nm}}$ ratio having implications for a dynamic structure, relative to the WT protein. Based on helical-helical interactions within coiled-coil systems, a $\theta_{222/208 \text{ nm}}$ ratio of > 1.1 is indicative of quaternary structure formation (i.e. two α-helical monomers interacting) with $\theta_{222/208 \text{ nm}}$ ratios of 0.9 or less being indicative of isolated helices.[65-67] Moreover for helical proteins, the $\theta_{222/208 \text{ nm}}$ ratio can be associated with interhelical contacts and therefore can provide low-resolution information as to whether mutations cause a 'loosening' of the structure.[49] Based on our previous NMR studies to probe main chain dynamics in the WT protein and the G41S and Y48H variants,[5, 31] the $\theta_{222/208 \text{ nm}}$ ratios appear to correlate, in that the G41S was determined by NMR to be more dynamic than the WT, but less dynamic than the Y48H variant. Therefore based on the $\theta_{222/208 \text{ nm}}$ ratio we suggest under non-denaturing conditions that the A51V variant is closer dynamically to the G41S variant than the Y48H variant.

The *m*-value from chemical denaturation experiments is generally considered to give an estimate of the compactness or the degree of residual structure in the denatured state.[68, 69] Table 1 reveals the *m*-value for the WT and variants decreases in the order WT > A51V $\cong$ G41S > Y48H. In yeast iso-1-Cc the *m*-value for the K54H variant is decreased relative to the WT protein [70] and this has been attributed to ligation by the His to the heme in the denatured state constraining the polypeptide and causing a more compact denatured state.[70] Neither the A51V or the G41S variants have substitutions that can coordinate the heme, yet in both cases the *m*-values decrease and notably more so than for substitutions in the 71-85 Ω-loop of hCc.[25] Thus the substitutions at the 41 and 51 positions contribute to destabilizing the 40-57 Ω-loop (the lowest energy foldon of Cc), resulting in a more compact denatured state. A similar suggestion may be put forward for the Y48H variant, particularly now that by introducing a His this variant may behave similarly to the K54H variant of yeast iso-1 Cc.[70] However, the *m*-value for the Y48H variant is further decreased in respect to the A51V and G41S variants.[5] Solution state NMR studies under non-denaturing conditions with the Y48H variant are consistent with the presence of a partially unfolded form populated under non-denaturing conditions that bears the hallmarks of having an unfolded α2-helix.[5] The *m*-value can also

infer the occurrence of intermediates on the unfolding pathway.[71-73] For example, the decreased *m*-value of the K73H variant of yeast iso-1 Cc was not ascribed to His-heme ligation in the denatured state as for the K54H variant,[70] but rather to the existence of a native-like unfolding intermediate at low denaturant concentrations.[72] Notably, solution NMR studies with the G41S variant, albeit indicative of increased dynamics relative to WT hCc,[31] are not consistent with a partially unfolded state populated under non-denaturing conditions. Therefore, it is likely that the *m*-value for the G41S and the A51V variants reflect more compact denatured states, whereas the much lower *m*-value determined for the Y48H variant is consistent with the presence of a native-like intermediate accessible under non-denaturing conditions, with consequences for peroxidase activity.

The Met80-off rate for the A51V variant estimated from N_3^- binding kinetics lies between the WT hCc and the G41S variant (Table 1). The ratio $^{WT}K_{app}/^{variant}K_{app}$ reflects the ratio of equilibrium constants for dissociation and reassociation of the Met80 ligand ($^{variant}K/^{WT}K$). Thus based on the low K_{app} (high affinity for N_3^-) for the A51V variant the $^{WT}K_{app}/^{A51V}K_{app}$ is identical to the ratio for the Y48H variant indicating that the K values are similar and hence the population of the pentacoordinate forms in these two variants at equilibrium are equivalent. In spite of this, the peroxidase activity, while enhanced for the A51V variant is not at the Y48H level,[5] or for that matter the G41S variant,[5] where from the ratio of $^{WT}K_{app}/^{G41S}K_{app}$ the population of the G41S pentacoordinate form is lower.[31] Therefore, we suggest that the observed trend in peroxidase activity between variants is not purely a consequence of the population of the pentacoordinate form, but rather the rate constant (*i.e.* Met80-off rate, k_1) for accessing the pentacoordinate state is a dominant factor (k_1 values WT < A51V ≅ G41S < Y48H). In contrast, there is a lack of correlation between k_{f1} (the rate of formation of the alkaline form, Table 2) and k_1, albeit that the transition to the alkaline form must incorporate the step in which Met80 dissociates. This implies that the rate determining step in the alkaline transition is not the Met80-off rate but rather subsequent steps involving the conformational transition and Lys binding to the ferric heme.

Based on the above discussion the extent to which the native ferric hCc structure can facilitate peroxidase activity in these disease variants must be reconciled as an interplay between the Met80-off rate and tertiary structure dynamics. This view is further enhanced through recent studies with horse Cc using chemical denaturants to investigate peroxidase activity and ligand binding.[74] For the A51V and G41S variants the peroxidase activity whilst higher than WT hCc does not attain the Y48H variant levels, despite the pentacoordinate state

of the A51V variant being populated to the same extent as the Y48H variant. In the case of the latter the increased Met80-off rate and a highly dynamic solution state with ease of access to an unfolded state in which the 40-57 and 71-85 Ω-loops are highly perturbed[5] contribute to the higher peroxidase activity.

Further insight into the peroxidase function of the variants may be obtained from the kinetics of the alkaline transition and the mechanistic framework in which four pentacoordinate forms can in theory be populated and illicit peroxidase activity (see the four corners of the front face of the cube in Figure 9 of Deacon *et al.*[25]). For the A51V variant the pK_a and the pK_{H1} values are essentially the same as the G41S and Y48H variants, implying greater ease of access to the pCc-H species (Scheme 2). As a Lys will be more protonated at pH 6.5, where peroxidase assays were monitored, this pentacoordinate species (pCc-H) will be more populated at equilibrium than the WT hCc.

The interpretation of the second ionisation (pK_{H2}) of the alkaline transition in relation to peroxidase activity is more difficult. For the A51V variant the pK_{H2} value is higher by ~ 0.5 pH units than either the G41S and Y48H variants (Fig. 5C).[25] The group we and others have previously suggested to be responsible for stabilization of this HS form by deprotonation, is the proximal His18, which can lose a proton at high pH in the G41S and Y48H variants, but cannot do so in the WT hCc in the accessible pH range.[25] Bowler and colleagues have reported the existence of a water channel as a result of a repositioning of the 40-57 Ω-loop in a non-native state of Cc, allowing access to the proximal His18 ligand.[15] The pH profile in Figure 5C suggests that loss of a proton to the bulk solution is more difficult for the A51V variant than either the G41S or Y48H variants [25] yielding a higher pK_{H2}. Although the A51V and Y48H variants have similar fractions of the ferric protein in the pentacoordinate state, the ease of which these forms can be stabilized by deprotonation (Scheme 2 and the mechanistic scheme (cube in Fig. 9) reported in[25]) appears to be subtly different. An explanation for this could manifest from differences in dynamics on the proximal side of the heme. We note that the substitutions at the 41 and 48 positions are at a juxtaposition to the 20's Ω-loop compared to the 51 position (Fig. 1). It has been well documented that the disruption of a hydrogen-bond between His26 and Pro44 causes the subsequent release of the 20's and 40's Ω-loops leading to His18 being more accessible.[75] It could therefore be that the G41S and Y48H variants are more prominent than the A51V variant in perturbing this interaction and as a consequence instil a more dynamic proximal His side of the heme accounting for the subtilties in stabilizing the

HS form of the G41S and Y48H variants over the A51V variant, with consequences for H_2O_2 access.

Whilst extensive *in vitro* studies have been conducted on the hCc disease variants focusing on their apoptotic function, the effect of these mutations on respiratory chain function *in vitro* is lacking. From *in vivo* studies both the G41S and Y48H variants have been reported to induce a small defect in respiratory function based on measuring O_2 consumption in cellular assays.[39] However, these studies do not report on the steady-state ratio of ferric/ferrous Cc when in turnover with CcO, which from the present and previous studies would be expected to vary in the disease variants When oxidised hCc and its variants are initially in the acid ferric form, *i.e.* the hexacoordinate (His/Met) conformer that possesses a 695 nm absorption band. Thereafter the ferric protein comes into conformational equilibrium between the acid and alkaline forms, the proportions of which depend on the ambient pH and the apparent pK_a of the alkaline transition. The WT hCc has an apparent pK_a of 9.3 (Table 2) while all the disease associated variants have apparent pK_a values ~ 1 pH unit lower. Thus, at pH 7.4 (experimental pH of the turnover assay), approximately 1 % of the WT and 10 % of the variants should, at equilibrium, be in the alkaline form. This means that in turnover experiments, as illustrated in Fig. 7, there will be a thermodynamic driving force towards the ferric alkaline form (1 % WT and up to 10 % for the variants), which cannot be reduced by ascorbate until, in the dynamic equilibrium, it returns to the acid form that can be reduced. Similarly, *in vivo* reduction of the alkaline form by the bc_1 complex occurs at the rate of transition from alkaline to acid forms of Cc. The extent to which this happens is dependent not only on the pK_a for the alkaline transition but also on the electron flux through the respiratory chain, for example in circumstances in which the Cc is held in the ferrous state, then no alkaline form of the ferric protein is present. The experimental results are consistent with this expectation, except that not all the variants populate the alkaline form to the same extent (10 %, see above). This is because in the steady-state the ferric forms do not come into true equilibrium and the rate of approach to this equilibrium is variant dependant. The relaxation time (τ) of the equilibrium between the acid and alkaline forms *i.e.* $1/\tau = k_{f1} + k_{b1}$ is variant dependent and controls the kinetics of the approach to equilibrium and hence the extent to which the alkaline form is populated. These results therefore demonstrate that the disease related variants of hCc can have measurable effects on the mitochondrial electron-transfer system. The magnitude of any such effect must depend on the redox state of hCc and hence on the energetic state of the cell (*i.e.* coupled/uncoupled respiration) and on the time of residence of any given molecule of hCc in

the ferric state. These complex interactions cannot be readily assessed, but the overall effect of the 40-57 Ω-loop variants is clear. Thus, although not as important as the well documented effects such as enhanced peroxidase activity it is worth pointing out that such mutations may have small but possibly significant effects on the overall energetics of the cell. Within this context we see that A51V perturbs the redox state to a minor degree compared to the G41S and Y48H variants.

CONCLUSIONS

From *in vitro* studies all three hCc variants display physicochemical properties of the ferric form that influence peroxidase activity. The A51V variants displays features that we believe are consistent with a less dynamic native state than the Y48H variant, and is closer in dynamic properties to the G41S variant. Notably the A51V variant stands out in that despite having a population of the pentacoordinate form equal to the Y48H variant, peroxidase activity is the lowest of the three variants; a result we ascribe to the lower Met80 off-rate and subtle variations in main chain dynamics caused at the different mutation sites. The clinical features of the families expressing the G41S and Y48H variants both show similar reduced mean platelet counts with normal platelet volume and function.[76] However, the A51V family, whilst also displaying reduced mean platelet counts has in addition a platelet function defect.[76] Thus a distinction in clinical phenotypes between the G41S and Y48H variants versus the A51V variant is evident and may correlate to some of the physicochemical properties we elucidate here. The excursion into assessing the *in vitro* respiratory properties through monitoring the steady-state ratio of ferric/ferrous Cc when in turnover with CcO has illustrated that mitochondrial respiration can be compromised by mutations in the 40-57 Ω-loop, the effect being small, but depending on the respiratory state of the cell, possibly significant.

FUNDING

SUPPORTING INFORMATION

Figure S1 illustrative reaction time courses at 550 nm for human cytochrome *c* turnover with cytochrome *c* oxidase. Table S1 reports the extinction coefficient at 409 nm for human cytochrome *c* and the 40-57 Ω-loop variants.

REFERENCES

[1] Y.P. Ow, D.R. Green, Z. Hao, T.W. Mak, Nat. Rev. Mol. Cell Biol. 9 (2008) 532-542.

[2] M. Huttemann, P. Pecina, M. Rainbolt, T.H. Sanderson, V.E. Kagan, L. Samavati, J.W. Doan, I. Lee, Mitochondrion 11 (2011) 369-381.

[3] K. Gonzalez-Arzola, I. Diaz-Moreno, A. Cano-Gonzalez, A. Diaz-Quintana, A. Velazquez-Campoy, B. Moreno-Beltran, A. Lopez-Rivas, M.A. De la Rosa, Proc. Natl. Acad. Sci. U. S. A. 112 (2015) 9908-9913.

[4] D. Alvarez-Paggi, L. Hannibal, M.A. Castro, S. Oviedo-Rouco, V. Demicheli, V. Tortora, F. Tomasina, R. Radi, D.H. Murgida, Chem. Rev. 117 (2017) 13382-13460.

[5] O.M. Deacon, A.I. Karsisiotis, T. Moreno-Chicano, M.A. Hough, C. Macdonald, T.M.A. Blumenschein, M.T. Wilson, G.R. Moore, J.A.R. Worrall, Biochemistry 56 (2017) 6111-6124.

[6] R. Santucci, F. Sinibaldi, P. Cozza, F. Polticelli, L. Fiorucci, Int. J. Biol. Macromol. 136 (2019) 1237-1246.

[7] G.R. Moore, G.W. Pettigrew, Cytochrome c: Evolutionary, Structural and Physicochemical Aspects, Springer-Verlag, London, 1990.

[8] J.F. Leszczynski, G.D. Rose, Science 234 (1986) 849-855.

[9] J.S. Fetrow, FASEB J. 9 (1995) 708-717.

[10] R. Radi, L. Thomson, H. Rubbo, E. Prodanov, Arch. Biochem. Biophys. 288 (1991) 112-117.

[11] M.A. Rosei, C. Blarzino, R. Coccia, C. Foppoli, L. Mosca, C. Cini, Inter. J. Biochem. Cell Biol. 30 (1998) 457-463.

[12] R. Vazquez-Duhalt, J. Mol. Catal. B-Enzym. 7 (1999) 241-249.

[13] R.E. Diederix, M. Ubbink, G.W. Canters, Eur. J. Biochem. 268 (2001) 4207-4216.

[14] R.E. Diederix, M. Ubbink, G.W. Canters, Biochemistry 41 (2002) 13067-13077.

[15] L.J. McClelland, T.C. Mou, M.E. Jeakins-Cooley, S.R. Sprang, B.E. Bowler, Proc. Natl. Acad. Sci. U. S. A. 111 (2014) 6648-6653.

[16] V.E. Kagan, V.A. Tyurin, J. Jiang, Y.Y. Tyurina, V.B. Ritov, A.A. Amoscato, A.N. Osipov, N.A. Belikova, A.A. Kapralov, V. Kini, Vlasova, II, Q. Zhao, M. Zou, P. Di, D.A. Svistunenko, I.V. Kurnikov, G.G. Borisenko, Nat Chem Biol, vol. 1, 2005, pp. 223-232.

[17] N.A. Belikova, Y.A. Vladimirov, A.N. Osipov, A.A. Kapralov, V.A. Tyurin, M.V. Potapovich, L.V. Basova, J. Peterson, I.V. Kurnikov, V.E. Kagan, Biochemistry 45 (2006) 4998-5009.

[18] A.A. Kapralov, I.V. Kurnikov, Vlasova, II, N.A. Belikova, V.A. Tyurin, L.V. Basova, Q. Zhao, Y.Y. Tyurina, J. Jiang, H. Bayir, Y.A. Vladimirov, V.E. Kagan, Biochemistry 46 (2007) 14232-14244.

[19] J. Hanske, J.R. Toffey, A.M. Morenz, A.J. Bonilla, K.H. Schiavoni, E.V. Pletneva, Proc. Natl. Acad. Sci. U. S. A. 109 (2012) 125-130.

[20] A. Patriarca, F. Polticelli, M.C. Piro, F. Sinibaldi, G. Mei, M. Bari, R. Santucci, L. Fiorucci, Arch. Biochem. Biophys. 522 (2012) 62-69.

[21] B.S. Rajagopal, G.G. Silkstone, P. Nicholls, M.T. Wilson, J.A. Worrall, Biochim. Biophys. Acta 1817 (2012) 780-791.

[22] J. Muenzner, J.R. Toffey, Y. Hong, E.V. Pletneva, J. Phys. Chem. B 117 (2013) 12878-12886.

[23] B.S. Rajagopal, A.N. Edzuma, M.A. Hough, K.L. Blundell, V.E. Kagan, A.A. Kapralov, L.A. Fraser, J.N. Butt, G.G. Silkstone, M.T. Wilson, D.A. Svistunenko, J.A. Worrall, Biochem. J. 456 (2013) 441-452.

[24] T.M. Josephs, I.M. Morison, C.L. Day, S.M. Wilbanks, E.C. Ledgerwood, Biochem. J. 458 (2014) 259-265.

[25] O.M. Deacon, D.A. Svistunenko, G.R. Moore, M.T. Wilson, J.A.R. Worrall, Biochemistry 57 (2018) 4276-4288.

[26] X.L. Hong, D.W. Dixon, FEBS Lett. 246 (1989) 105-108.

[27] J.C. Ferrer, J.G. Guillemette, R. Bogumil, S.C. Inglis, M. Smith, A.G. Mauk, J. Am. Chem. Soc. 115 (1993) 7507-7508.

[28] F.I. Rosell, J.C. Ferrer, A.G. Mauk, J. Am. Chem. Soc. 120 (1998) 11234-11245.

[29] E. Margoliash, A. Schejter, Advs. Prot. Chem. 21 (1966) 113-286.

[30] M.T. Wilson, C. Greenwood, in: R.A. Scott & A.G. Mauk (Ed.), Cytochrome c: A multidiscipinary approach, University Science Books 1996.

[31] A.I. Karsisiotis, O.M. Deacon, M.T. Wilson, C. Macdonald, T.M. Blumenschein, G.R. Moore, J.A. Worrall, Sci. Rep. 6 (2016) 30447.

[32] H. Maity, J.N. Rumbley, S.W. Englander, Proteins, vol. 63, 2006, pp. 349-355.

[33] M.M. Krishna, Y. Lin, J.N. Rumbley, S.W. Englander, J. Mol. Biol. 331 (2003) 29-36.

[34] H. Maity, M. Maity, M.M. Krishna, L. Mayne, S.W. Englander, Proc. Natl. Acad. Sci. U. S. A. 102 (2005) 4741-4746.

[35] M.M. Krishna, H. Maity, J.N. Rumbley, Y. Lin, S.W. Englander, J. Mol. Biol. 359 (2006) 1410-1419.

[36] W. Hu, Z.Y. Kan, L. Mayne, S.W. Englander, Proc. Natl. Acad. Sci. U. S. A. 113 (2016) 3809-3814.

[37] M.W. Mara, R.G. Hadt, M.E. Reinhard, T. Kroll, H. Lim, R.W. Hartsock, R. Alonso-Mori, M. Chollet, J.M. Glownia, S. Nelson, D. Sokaras, K. Kunnus, K.O. Hodgson, B. Hedman, U. Bergmann, K.J. Gaffney, E.I. Solomon, Science 356 (2017) 1276-1280.

[38] I.M. Morison, E.M. Cramer Borde, E.J. Cheesman, P.L. Cheong, A.J. Holyoake, S. Fichelson, R.J. Weeks, A. Lo, S.M. Davies, S.M. Wilbanks, R.D. Fagerlund, M.W. Ludgate, F.M. da Silva Tatley, M.S. Coker, N.A. Bockett, G. Hughes, D.A. Pippig, M.P. Smith, C. Capron, E.C. Ledgerwood, Nat. Genet. 40 (2008) 387-389.

[39] D. De Rocco, C. Cerqua, P. Goffrini, G. Russo, A. Pastore, F. Meloni, E. Nicchia, C.T. Moraes, A. Pecci, L. Salviati, A. Savoia, Biochim. Biophys. Acta 1842 (2014) 269-274.

[40] B. Johnson, G.C. Lowe, J. Futterer, M. Lordkipanidze, D. MacDonald, M.A. Simpson, I. Sanchez-Guiu, S. Drake, D. Bem, V. Leo, S.J. Fletcher, B. Dawood, J. Rivera, D. Allsup, T. Biss, P.H. Bolton-Maggs, P. Collins, N. Curry, C. Grimley, B. James, M. Makris, J. Motwani, S. Pavord, K. Talks, J. Thachil, J. Wilde, M. Williams, P. Harrison, P. Gissen, S. Mundell, A. Mumford, M.E. Daly, S.P. Watson, N.V. Morgan, Haematologica 101 (2016) 1170-1179.

[41] Y. Uchiyama, K. Yanagisawa, S. Kunishima, M. Shiina, Y. Ogawa, M. Nakashima, J. Hirato, E. Imagawa, A. Fujita, K. Hamanaka, S. Miyatake, S. Mitsuhashi, A. Takata, N. Miyake, K. Ogata, H. Handa, N. Matsumoto, T. Mizuguchi, Clin. Gen. 94 (2018) 548-553.

[42] M.D. Liptak, R.D. Fagerlund, E.C. Ledgerwood, S.M. Wilbanks, K.L. Bren, J. Am. Chem. Soc. 133 (2011) 1153-1155.

[43] T.M. Josephs, M.D. Liptak, G. Hughes, A. Lo, R.M. Smith, S.M. Wilbanks, K.L. Bren, E.C. Ledgerwood, J. Biol. Inorg. Chem. 18 (2013) 289-297.

[44] T. Yonetani, J. Biol. Chem. 235 (1960) 845-852.

[45] E.A. Berry, B.L. Trumpower, Anal. Biochem. 161 (1987) 1-15.

[46] M.M. Santoro, D.W. Bolen, Biochemistry 31 (1992) 4901-4907.

[47] J.M. Mason, D.S. Bendall, C.J. Howe, J.A. Worrall, Biochim. Biophys. Acta 1824 (2012) 311-318.

[48] H. Lei, B.E. Bowler, J. Phys. Chem. B 123 (2019) 8939-8953.

[49] G.E. Arnold, L.A. Day, A.K. Dunker, Biochemistry 31 (1992) 7948-7956.

[50] K.M. Black, I. Clark-Lewis, C.J. Wallace, Biochem, J. 359 (2001) 715-720.

[51] N. Sutin, J.K. Yandell, J. Biol. Chem. 247 (1972) 6932-6936.

[52] H.A. Harbury, J.R. Cronin, M.W. Fanger, T.P. Hettinger, A.J. Murphy, Y.P. Myer, S.N. Vinogradov, Proc. Natl. Acad. Sci. U. S. A. 54 (1965) 1658-1664.

[53] H. Theorell, J. Am. Chem. Soc. 63 (1941) 1820-1827.

[54] L.A. Davis, A. Schejter, G.P. Hess, J. Biol. Chem. 249 (1974) 2624-2632.

[55] H. Kihara, S. Saigo, H. Nakatani, K. Hiromi, M. Ikeda-Saito, T. Iizuka, Biochim. Biophys. Acta 430 (1976) 225-243.

[56] H. Hasumi, Biochim. Biophys. Acta, 626 (1980) 265-276.

[57] L. Hoang, H. Maity, M.M. Krishna, Y. Lin, S.W. Englander, J. Mol. Biol. 331 (2003) 37-43.

[58] S.M. Nold, H. Lei, T.C. Mou, B.E. Bowler, Biochemistry 56 (2017) 3358-3368.

[59] S. Ferguson-Miller, G.T. Babcock, Chem .Rev. 96 (1996) 2889-2908.

[60] S. Yoshikawa, A. Shimada, Chem. Rev. 115 (2015) 1936-1989.

[61] M. Brunori, A. Colosimo, G. Rainoni, M.T. Wilson, E. Antonini, J. Biol. Chem. 254 (1979) 10769-10775.

[62] C.N. Pace, J.M. Scholtz, Biophys. J. 75 (1998) 422-427.

[63] J. Hermans, A.G. Anderson, R.H. Yun, Biochemistry 31 (1992) 5646-5653.

[64] R. Aurora, T.P. Creamer, R. Srinivasan, G.D. Rose, J. Biol. Chem. 272 (1997) 1413-1416.

[65] S.Y. Lau, A.K. Taneja, R.S. Hodges, J. Biol. Chem. 259 (1984) 13253-13261.

[66] S.C. Kwok, R.S. Hodges, J .Biol. Chem. 279 (2004) 21576-21588.

[67] N.E. Shepherd, H.N. Hoang, G. Abbenante, D.P. Fairlie, J. Am. Chem. Soc. 127 (2005) 2974-2983.

[68] D. Shortle, Advs. Prot. Chem. 46 (1995) 217-247.

[69] J.M. Scholtz, G.R. Grimsley, C.N. Pace, Meth. Enzymol. 466 (2009) 549-565.

[70] B.N. Hammack, C.R. Smith, B.E. Bowler, J. Mol. Biol. 311 (2001) 1091-1104.

[71] J.H. Carra, P.L. Privalov, FASEB J. 10 (1996) 67-74.

[72] S. Godbole, A. Dong, K. Garbin, B.E. Bowler, Biochemistry 36 (1997) 119-126.

[73] S. Godbole, B.E. Bowler, Biochemistry 38 (1999) 487-495.

[74] N. Tomaskova, R. Varhac, V. Lysakova, A. Musatov, E. Sedlak, Biochim. Biophys. Acta, 1866 (2018) 1073-1083.

[75] G. Balakrishnan, Y. Hu, T.G. Spiro, J. Am. Chem. Soc. 134 (2012) 19061-19069.

[76] E.C. Ledgerwood, C. Dunstan-Harrison, L. Ong, I.M. Morison, Platelets 30 (2019) 672-674.

Table 1: Summary of thermodynamic and kinetic parameters for ferric WT hCc and the three 40-57 Ω-loop variants determined by GuHCl denaturation (15 °C, 10 mM potassium phosphate, 50 mM potassium fluoride pH 6.5) and azide binding kinetics (25 °C, 50 mM MES pH 7.0).

GuHCl denaturation				
protein	ΔG_{unf} (kcal mol^{-1})	$\Delta\Delta G_{unf}$ (kcal mol^{-1})	m (kcal mol^{-1} M^{-1})	C_m (M)
A51V	6.99 ± 0.16	3.66 ± 0.71	3.02 ± 0.07	2.32 ± 0.05
G41S	6.75 ± 0.10[a]	3.90 ± 0.65	3.00 ± 0.10[a]	2.25 ± 0.05[a]
Y48H	5.09 ± 0.16[a]	5.56 ± 0.71	2.57 ± 0.10[a]	1.98 ± 0.05[a]
WT	10.65 ± 0.55[a]	-	4.10 ± 0.25[a]	2.60 ± 0.05[a]

Azide binding kinetics		
protein	K_{app} (M)	k_1 (s^{-1})	k_{-2} (s^{-1})
A51V	0.07 ± 0.06	33 ± 17[d]	7.6 ± 0.5[d]
G41S	0.11 ± 0.01[b]	45 ± 18[b]	8.9 ± 0.3[b]
Y48H	0.07 ± 0.01[a]	175 ± 94[c,d]	11.1 ± 1.1[c,d]
WT	0.31 ± 0.03[b]	5.77 ± 1.5[b]	3.5 ± 0.4[b]

[a]Values taken from ref. 5.
[b]Values taken from ref. 31.
[c]Data taken from ref. 5 and refitted in the present study.
[d]For the A51V and Y48H variants, k_{-2} has been fitted using equation 4, and thereafter fixed to determine the errors on k_1 (also using equation 4 with values reported in Table 1, see Materials and Methods). In addition, we have used the range of k_{-2} values reported in Table 1 to provide alternative commentary on the k_1 errors. Thus for the A51V variant the range of k_{-2} yielded values of $k_1 = 23 \pm 8$ s^{-1} (lower bound) and $k_1 = 64 \pm 79$ s^{-1} (upper bound). Likewise for the Y48H variant, $k_1 = 124 \pm 49$ s^{-1} (lower bound) and $k_1 = 329 \pm 318$ s^{-1} (upper bound). As k_{-2} and k_1 are hyperbolically related, then we see as expected values of k_{-2} approaching its asymptotic value of 11.8 ± 0.6 s^{-1} (see text), the error in k_1 becomes large i.e. near the asymptotic value of k_{-2}, small changes in k_{-2} lead to very large variation in k_1.

Table 2: Summary of parameters determined for the alkaline transition of ferric WT hCc and the three 40-57 Ω-loop variants.

	WT	A51V	G41S	Y48H
pK_a	9.3 ± 0.2[a]	8.3 ± 0.1	8.5 ± 0.2[a]	8.4 ± 0.1[a]
pK_{H1}	12.0 ± 0.4[b]	10.8 ± 0.1	10.5 ± 0.1[b]	10.4 ± 0.2[b]
k_{f1} (s^{-1})	17 ± 13[b]	8.3 ± 1.1	8.4 ± 1.3[b]	7.4 ± 1.4[b]
k_{b1} (s^{-1})[c]	0.034 ± 0.060	0.027 ± 0.012	0.084 ± 0.055	0.074 ± 0.051

[a]Data taken from ref. 5.
[b]Data taken from ref. 25.
[c]k_{b1} was calculated from K_c ($pK_c = pK_{H1} - pK_a$) as $k_{b1} = K_c k_{f1}$. The error on k_{b1} was calculated from the error on K_c (noting that $\sigma pK = 0.434(\sigma K_c/K_c)$) and the error on k_{f1} where $\sigma k_{b1} = K_c \sigma k_{f1} + k_{f1} \sigma K_c$
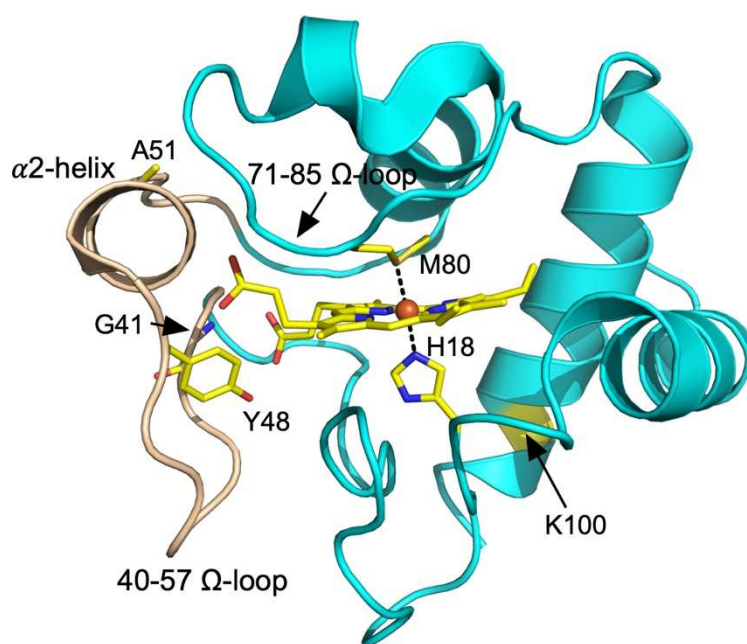
Figure 1: X-ray structure of hCc (3ZCF)[23] and the location of the THC4 causing variants. The 40-57 Ω-loop (beige) showing the three residues, Gly41, Tyr48 and Ala51, depicted in stick representation, that are mutated to Ser, His and Val, respectively. The position of Lys100 in the C-terminal helix is indicated in yellow. The heme and the axial iron ligands are shown in sticks and the 71-85 Ω-loop which communicates with the 40-57 Ω-loop is indicated.
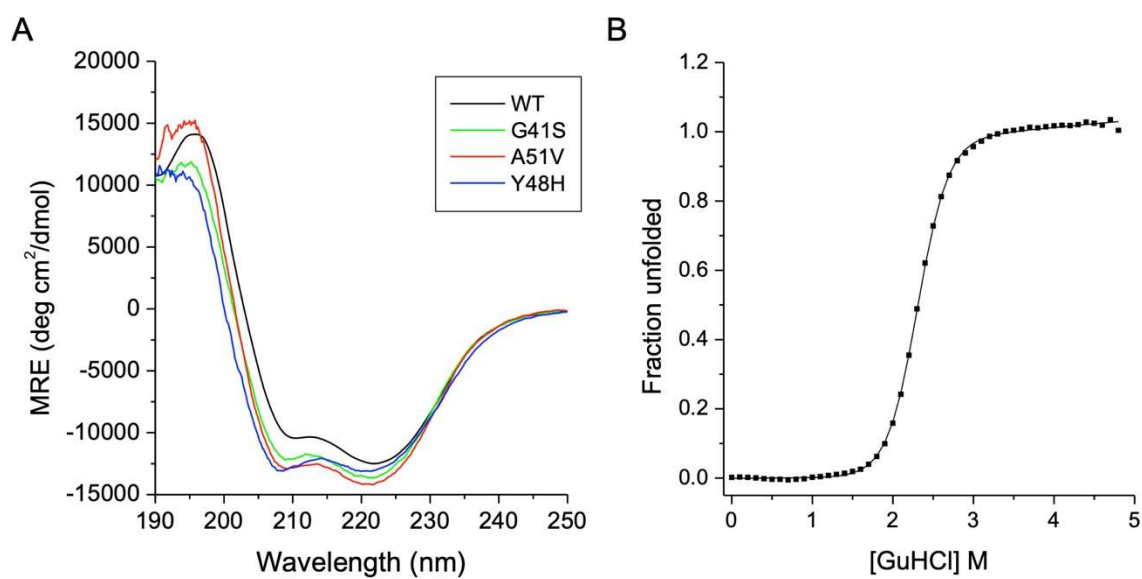
Figure 2: Far-UV CD spectroscopy and chemical denaturation. A) Far-UV CD profile of the ferric A51V variant of hCc compared to the profiles for the WT protein and the G41S and Y48H variants (pH 6.5 and 15 °C). B) Plot of the fraction unfolded versus GuHCl concentration for the ferric A51V hCc variant (pH 6.5, 15 °C) with the solid-line representing a fit to the data using a two-state equilibrium unfolding equation (see Materials and Methods). The determined thermodynamic parameters are reported in Table 1.
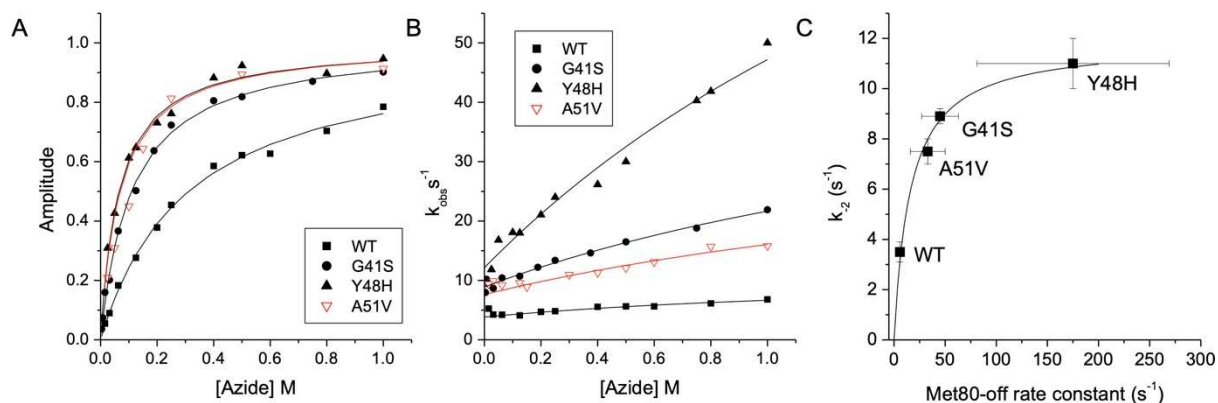
Figure 3: Azide binding to the ferric A51V variant of hCc compared with data for the WT protein and G41S and Y48H variants[23, 31] at pH 7.0 and 25 $^{\circ}$C. A) Amplitude changes from the reaction time-courses obtained using stopped-flow absorption spectroscopy at 420 nm plotted against azide concentration. Data are fitted to a hyperbola to yield K_{app} values reported in Table 1. B) Rate constants (k_{obs}) determined for azide binding with solid lines representative of fits to equation 4 with k_1 and k_{-2} values reported in Table 1. C) The relationship between the azide dissociation rate constant (k_{-2}) and the Met80-off rate (k_1) with the line through the points fitted to a hyperbola.
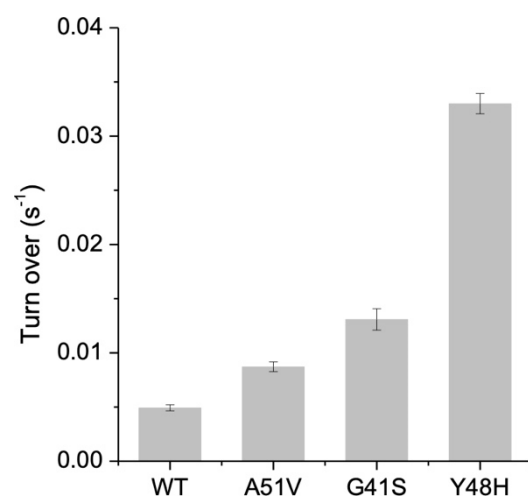
Figure 4: Peroxidase activity at pH 6.5. The maximum peroxidation rates of ABTS with the various forms of ferric Cc. The error bars are the standard error from measurements carried out in triplicate.
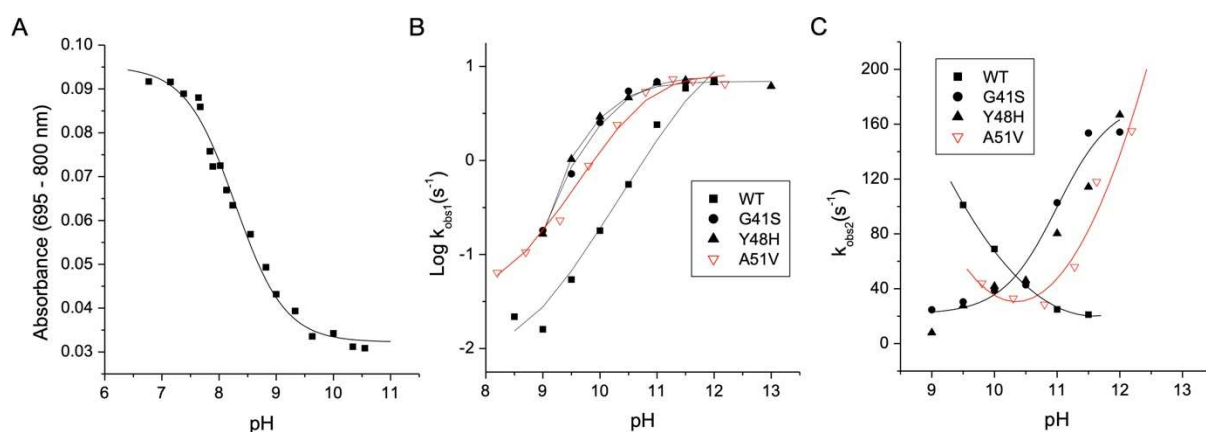
Figure 5: The alkaline transition of the ferric A51V variant. A) The decrease in absorbance at 695 nm plotted as a function of pH, with the solid-line representative of a fit to the data using a one-proton equilibrium equation with apparent pK_{695} values reported in Table 2. B) The pH dependence of k_{obs1} for the slow phase of the alkaline transition for WT hCc and the three 40-57 Ω-loop variants determined from pH jump experiments. The lines are fits to the logarithmic transformation of equation 5 to yield the pK_{H1} (Table 2). C) The pH dependence of k_{obs2} for the alkaline transition plotted as a function of pH. The solid lines through the data points for hCc, and the A51V variant indicates the trends in the data, whereas for the G41S and Y48H variants the solid line represents a combined fit to a one-proton equilibrium equation to yield pK_{H2}.
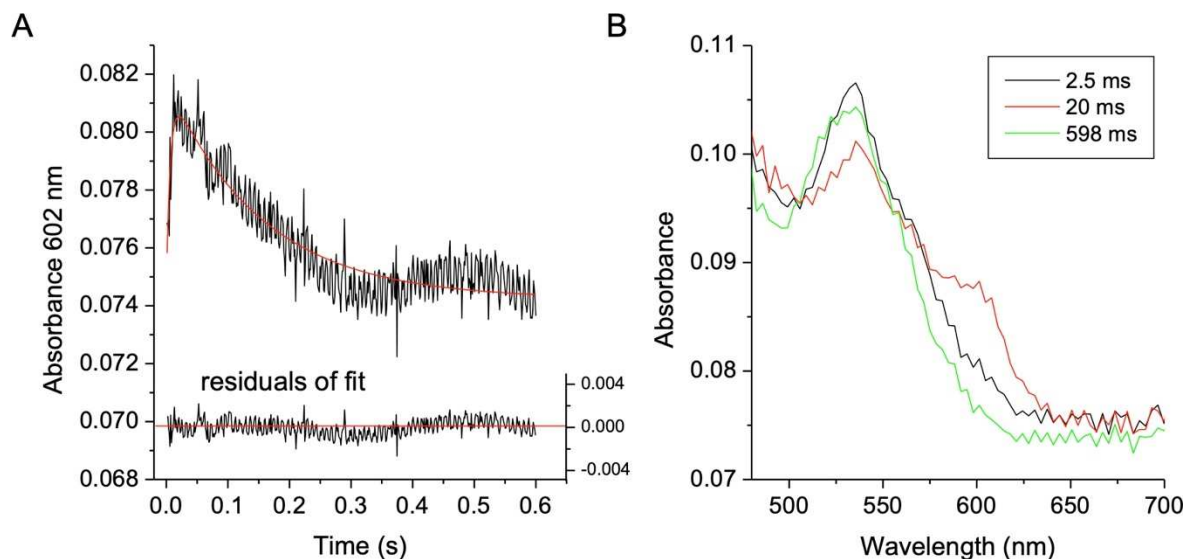
Figure 6: pH jump kinetics for the fast phase of the ferric A51V hCc variant at pH > 10.5. A) Single wavelength stopped-flow trace together with fit to a double-exponential on mixing ferric A51V hCc (pH 7) with an equal volume of a pH 11 buffer. The residuals of the double-exponential fit are illustrated. B) Optical transitions between 480 and 700 nm from stopped-flow spectroscopy taken at the indicated time during the pH jump experiment initiated as in (A). At $t = 2.5$ ms the spectrum represents the ferric hexacoordinate A51V variant, at $t = 20$ ms, the HS pentacoordinate form and at $t = 598$ ms the final His/Lys alkaline form.
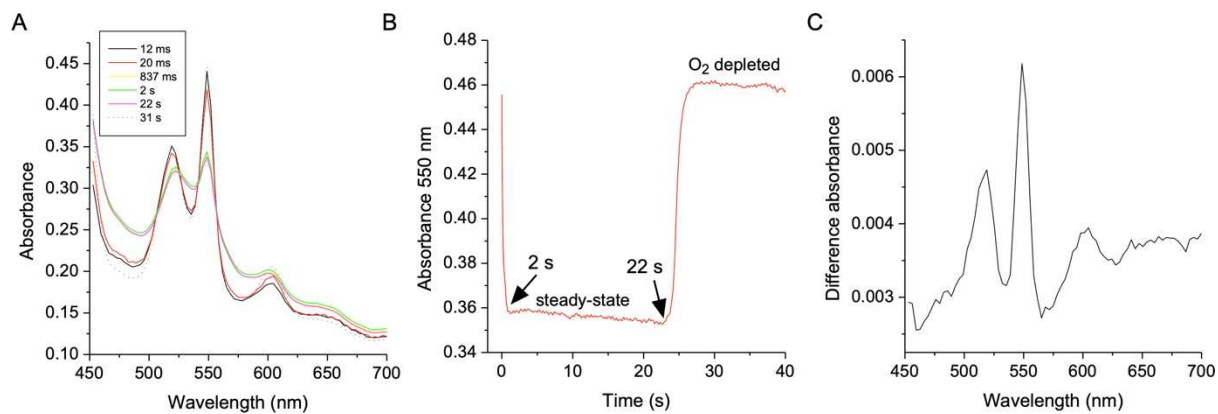
Figure 7: Redox states of hCc in turnover with CcO. A) Spectra collected at indicated times for the reactions of hCc (10 µM) in the presence of CcO (2.5 µM heme *a*), ascorbate (5 mM), TMPD (118 µM) and 135 µM oxygen (all concentrations after mixing), pH 7.4 and 25 °C. B) The time course collected at 550 nm (α-band of ferrous hCc) showing the approach to steady-state, and exit from steady-state. C) Difference spectrum between spectra taken at 2 s and 22 s (see B).
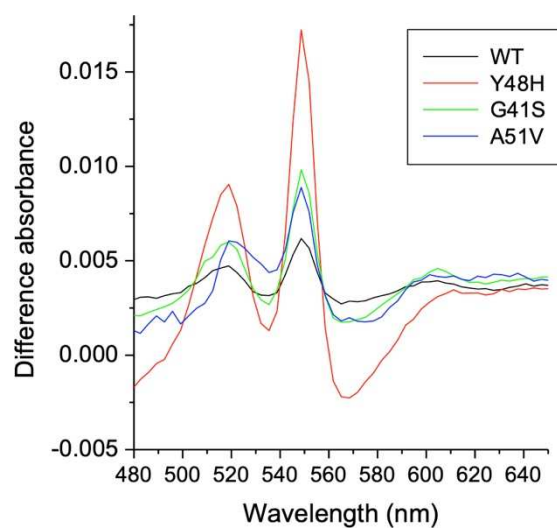
Figure 8: Comparison of difference spectra (2 s - 22 s) collected at pH 7.4 and 25 °C for the WT hCc and disease related variants. Each variant spectrum was normalised to a WT spectrum taken on the same day under the same conditions. The spectra have been adjusted to give the same absorbance at 700 nm.